Int J Adv Manuf Technol (2011) 52:451–461
DOI 10.1007/s00170-010-2756-6

ORIGINAL ARTICLE

# The effect of manufacturing variables on the corrosion resistance of a super duplex stainless steel

**A. M. Elhoud · N. C. Renton · W. F. Deans**

Received: 5 January 2010 / Accepted: 27 May 2010 / Published online: 29 June 2010
© Springer-Verlag London Limited 2010

**Abstract** Recent in-service failures of super duplex stainless steel (SDSS) components have revealed the important role of manufacturing variables on the corrosion behaviour of the material. These variables include surface condition, heat treatment and cold work. The effect of all three variables on the corrosion behaviour of an example SDSS was investigated using electrochemical techniques, tensile testing and microscopic observations. The role of surface condition was investigated by characterising the topography of specimens using the surface roughness parameter, $R_a$, then measuring the critical pitting temperature. The results showed that $R_a$ on its own is not sufficient to characterise the effect of surface condition on corrosion resistance. The effect of heat treatment on pitting potential was pronounced as a result of the intermetallic phases precipitated. Plastic deformation caused by cold work affected the pitting potential of the material, although the effects varied with increasing cold work; certain plastic strain levels caused reduced resistance, whilst others caused little change compared with the solution-annealed specimens. Hydrogen embrittlement increased with increasing cold work. The main conclusion is that the interactions between corrosive environments and SDSS components containing one or more of these manufacturing variables must be considered if reductions in service life are to be avoided.

**Keywords** Super duplex stainless steel · Surface condition · Inter-metallic · Cold work · Pitting corrosion · Hydrogen embrittlement

A. M. Elhoud (✉) · N. C. Renton · W. F. Deans
School of Engineering, University of Aberdeen,
AB24 3UE Aberdeen, UK
e-mail: a.alhoud@abdn.ac.uk

N. C. Renton
e-mail: n.c.renton@abdn.ac.uk

W. F. Deans
e-mail: w.f.deans@abdn.ac.uk

**Nomenclature**

| | |
|---|---|
| $R_a$ | Surface roughness (μm) |
| CPT | Critical pitting temperature (°C ) |
| $E_p$ | Pitting potential (mV Ag/AgCl) |
| $\varepsilon_{pl}$ | Plastic strain |

## 1 Introduction

In recent years, critical engineering components made from stainless steel have experienced a number of in-service failures across a range of industries. Subsequent investigations have reported that the failures, mainly environmentally assisted cracking, have initiated at sites affected by manufacturing issues which then became active when exposed to aggressive environments and operational events [1–5]. During manufacture, stainless steel engineering components pass through a number of different processes. These stages can be considered as manufacturing variables which affect the mechanical and corrosion resistance properties. Random variation during manufacture can result in changes in individual component properties and potentially defects, in the form of inclusions, plastic deformation or intermetallic precipitation as examples. These manufacturing variables all played some role in the failures described [5, 6], and further understanding of the phenomena involved would be of benefit in the development of manufacturing techniques for specific grades.

The duplex grades of stainless steel are a family of corrosion-resistant alloys that play an important role in industries where high stresses and severe environments are expected. The duplex grades are a dual-phase austenite/ferrite steel alloy with a nominal ferrite volume fraction of 50%. There are a variety of duplex grades with typical weight per cent chemical compositions of (22–25)Cr (0–3.5)Mo (0–2)W for corrosion resistance and (6–7)Ni (0.1–0.35)N for strength and toughness. The

chemical composition is used along with the pitting resistance equivalence number (PREN) to differentiate between the grades [7–9]. Those with PREN > 40 are known as "super" duplex stainless steel (SDSS).

The surface condition of SDSS components is one example of a manufacturing variable which has a significant effect on their corrosion resistance. The topography of the surface has an important influence on the corrosion mechanism through diffusion control which can cause localised corrosion initiation in less aggressive environments [6–12]. Characterisation and prediction of the final surface topography are therefore important when considering the manufacturing route for SDSS components [13–16]. Microstructural changes due to heat treatment are a second manufacturing variable that influences the properties of duplex stainless steels [17]. Improper heat treatment can produce harmful phases and disturb the structure of the austenitic/ferritic microstructure, resulting in premature failure of the components affected [18, 19]. The phases generated reduce both corrosion resistance and mechanical properties of SDSS by depleting the surrounding grains of the more noble elements (Cr, Mo, W), leaving them susceptible to attack. Some of the phases, particularly sigma phase, are also very brittle and act as stress concentrators in the microstructure under applied load [8, 9, 20–23].

Plastic deformation induced by cold work is a third manufacturing variable of interest. To avoid harmful precipitates caused by heat treatment, duplex stainless steels are hardened by cold work. For seamless tubes of the kind of interest to the nuclear and oil and gas industries, this is achieved by a range of cold drawing, pilgering and floating mandrill techniques. The application of cold work introduces a number of metallurgical changes in the material including dislocations, twins, deformation bands, cell structures and emerging slip steps at the surfaces, all of which can have a significant effect on corrosion and hydrogen embrittlement mechanisms [24–26]. The deformation structures influence the surface topography, and hence diffusion characteristics at initiation, and the quality and thickness of the passive oxide film, and hence the resistance to localised corrosion attack and hydrogen uptake [27, 28], and introduce dislocations and traps within the subsurface that enhance hydrogen embrittlement mechanisms [29]. Specific cold work treatments create specific deformation structures, and excessive cold work can lead to failure in suitable environments [30].

The failures described and the complex chemical composition and microstructure of the duplex grades make them particularly sensitive to the effects of these manufacturing variables. Most producers of SDSS grades use different manufacturing routes and technologies to meet the same requirements of international standards. This can mean that even the same nominal grades of duplex can have different mechanical and corrosion resistance properties if made by different manufactures. In this study, each of the variables described (surface condition, heat treatment and cold work) was investigated to give new insight into the effect on the mechanical and corrosion resistance properties of a specific super duplex stainless steel grade.

## 2 Experimental work procedures

Specimens were taken from a UNS S39274 super duplex stainless steel tubular with chemical composition in weight per cent: 0.02% C, 0.45% Mn, 24.84% Cr, 6.54% Ni, 3.10% Mo, 2.07% W, 0.28% N and rest per cent Fe. The specimens for the critical pitting temperature (CPT) tests were taken from three different regions on the SDSS tubular representing different manufacturing surface conditions. Examples of typical mill surface, heavy and light grinding surfaces were taken. The surface roughness ($R_a$) was measured for each specimen using a Taylor–Hobson Talysurf. The mill surface had a surface roughness value $R_a$ = 3.5 μm, the two surfaces treated by disk grinding $R_a$ = 2.8 and 3.2 μm, respectively. The three manufacturing surfaces were compared with an artificial 600-grit paper surface with $R_a$ = 0.25 μm. The effect of $R_a$ on corrosion resistance was then evaluated using the CPT of each specimen according to ASTM G 150 electrochemical technique [31]. Electrochemical measurements of the critical pitting temperature were performed in 3.5% NaCl solution using a computer-controlled 263A Princeton Applied Research potentiostat. The electrochemical corrosion cell used in the study consists of a working electrode, an Ag/AgCl reference electrode and a platinum counter electrode. These electrodes were immersed in test solution in a polymer container. Potentiostatic tests at +700 mV Ag/AgCl enabled the extent of anodic current transfer as a function of

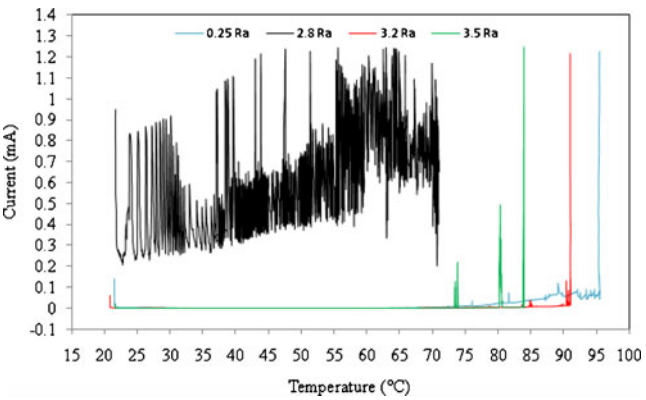


**Fig. 1** Critical pitting temperature results vs surface roughness, $R_a$ (μm)

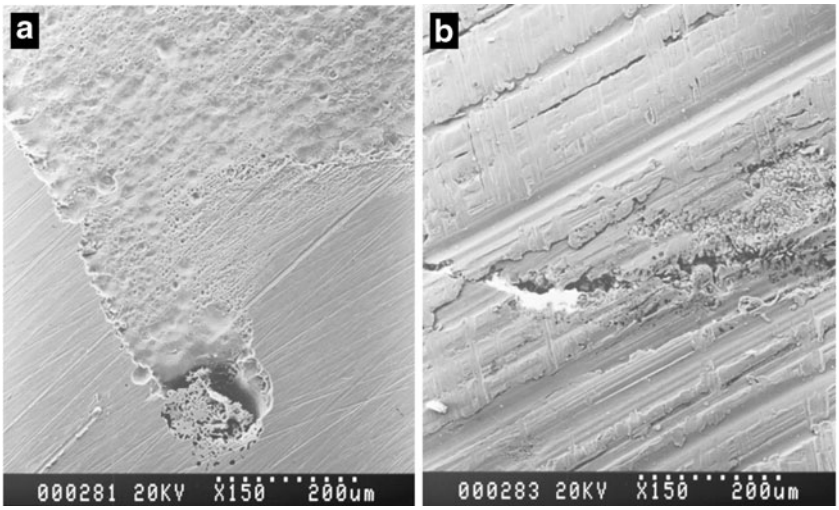


**Fig. 2** Corrosion morphologies on the SDSS surfaces after the electrochemical critical pitting temperature corrosion test ASTM G150: **a** $R_a$ = 0.25 μm, **b** $R_a$ = 2.8 μm

temperature to be determined. At the onset of corrosion, a continuously increasing current is recorded, and the temperature at which this happens is denoted the CPT [31, 32].

Heat treatment of the specimens was carried out at two different temperatures (1,000 and 1,300°C) for 30 min with two separate cooling regimes: water quench (WQ) and slower air cooling (AC). Identification of phase precipitation morphology and chemical composition was investigated using backscattered electron microscopy (BSE), scanning electron microscopy (SEM) and energy-dispersive X-ray spectroscopy (EDX). The effect of the heat treatment on corrosion resistance was again investigated using the potentiostat and the cyclic polarisation method. The potential scan for corrosion tests started from 100 mV below the free corrosion potential at a constant sweep rate of 1 mV/s. The pitting potential was denoted as the potential where the current reached 1 mA. The sweep scan reversed automatically at a current value of 3 mA. The protection potential was measured where the reverse curve crossed the initial passivity line. Three specimens per treatment group were carried out and the results averaged.

The effect of cold work on corrosion resistance was investigated using cylindrical specimens, initially 5 mm in diameter and 100 mm in length, strained in the axial direction at a slow strain rate of 0.1 mm/min beyond the elastic limit and into the plastic deformation range, allowing deformation structures to form on the external surface. Five different specimen types were created by applying different amounts of plastic strain ($\varepsilon_p$), namely 4%, 8%, 12% and 16%, in addition to solution-annealed specimens which were left unstrained. The effect of the external surface deformations was investigated by sectioning a set of the specimens and cold-mounting the sectioned surface before polishing to a mirror finish with a three-stage 240 grit/diamond paste/alumina suspension process. The corrosion resistance of all specimens in a 3.5 wt.% NaCl solution at 90°C was determined using the electrochemical pitting potential procedure described above.

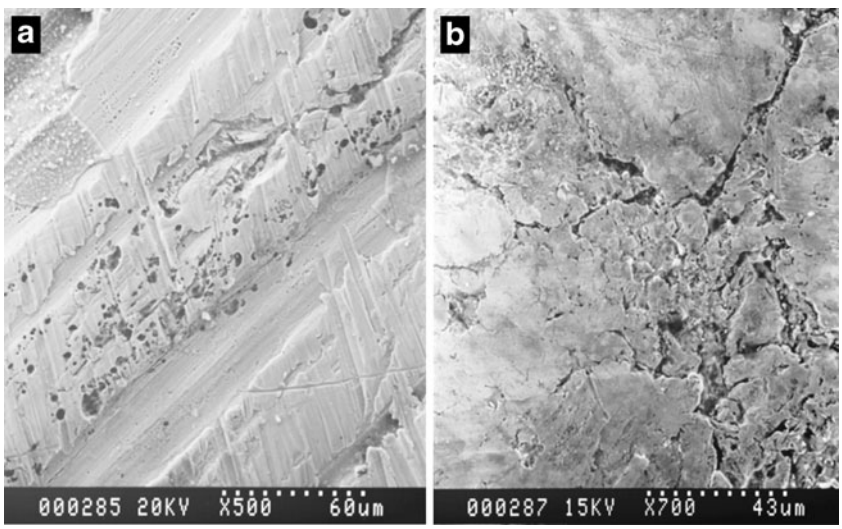


**Fig. 3** Corrosion morphologies on the SDSS surfaces after the electrochemical critical pitting temperature corrosion test ASTM G150: **a** $R_a$ = 3.2 μm, **b** $R_a$ = 3.5 μm

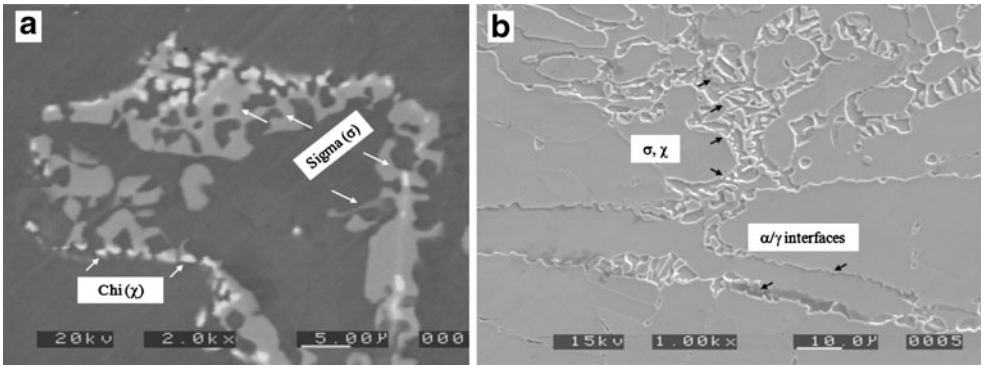


**Fig. 4** Photograph after 1,000°C for 30 min + WQ specimens: **a** BSE without chemical etching, **b** SEM after chemical etching

Hydrogen charging was carried out using a cathodic charging cell which consisted of a power supply controlling the applied current, platinum electrode connected to the positive lead in the power supply, and the tested sample connected to the negative lead at the power supply was applied. The working electrode of super duplex stainless steel was cathodically charged at a constant current of 30 mA/cm$^2$ for 48 h in solution containing 0.1 M $H_2SO_4$ with 10 mg/L of arsenic oxide. Charged and non-charged specimens were then strained to failure in air in an axial tensile test at a strain rate of 1 mm/min.

## 3 Results and discussion

### 3.1 Surface condition variable

The critical pitting temperature results of the various manufacturing surfaces are shown in Fig. 1. The curves exhibit typical electrochemical behaviour for the technique with a degree of stability in the current prior to the CPT. The 600-grit specimen with the lowest surface roughness of 0.25 µm showed the highest critical pitting temperature of around 95°C. The 2.8-µm surface showed immediate corrosion damage at the start temperature of 22°C. The 3.2- and 3.5-µm surface roughness specimens showed critical pitting temperature of around 90°C and 85°C, respectively. The results for the $R_a$ = 0.25-, 3.2- and 3.5-µm specimens confirmed the trend stated elsewhere that as the surface roughness increases, the corrosion resistance decreases [10, 33, 34]. The surface of the heavily ground specimen with $R_a$ = 2.8 µm is clearly outwith this trend. This is due to the ability of the deep narrow grooves on the ground surface to maintain an aggressive corrosive environment at the pit initiation site, leading to the early breakdown of the passive film. The geometry of the surface grooves makes it harder for metal ions ($M^+$) being released at the pit initiation site to move attracting negative chlorine ions to the site. The corrosion reaction in the presence of chloride ions produces hydrochloric acid (HCl), leading to a reduction in the pH at initiation sites near the bottom of the surface grooves. The net result is that the corrosion reaction becomes stable at lower potentials [10].

The morphology of the corrosion damage highlighted the difference in the surface profiles of the various specimens and the important role of surface topography on the corrosion mechanism. The 600-grit specimens with $R_a$ = 0.25 µm showed lacelike corrosion pits on the relatively uniform surface as shown in Fig. 2a. The surface of the heavy grinding specimen shown in Fig. 2b confirms the

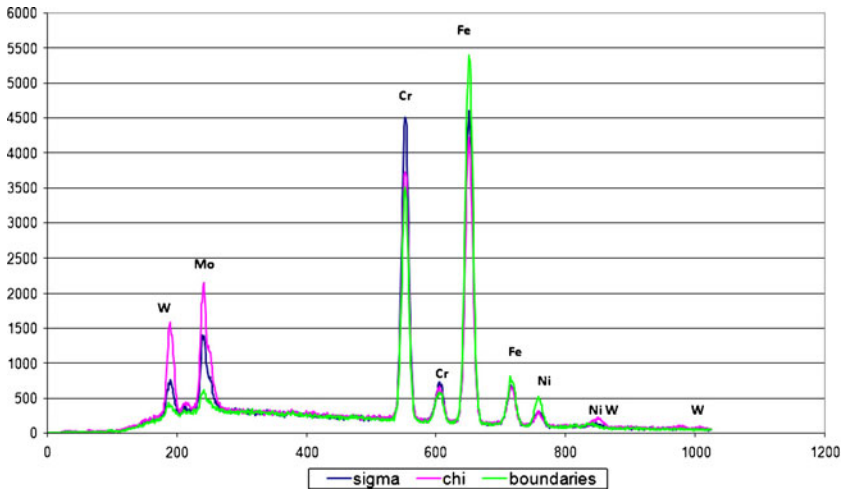


**Fig. 5** EDX analyses at the intermetallics and the ferrite/austenite boundaries of 1,000°C for 30 min+WQ specimens

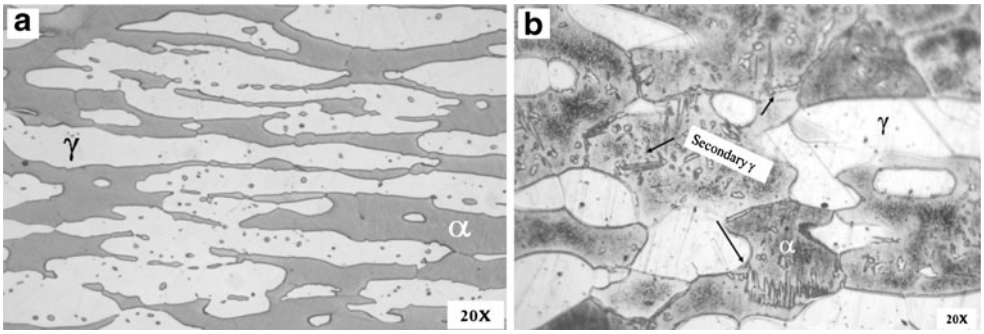


**Fig. 6** Metallographic of SDSS: **a** as received, **b** 1,300°C for 30 min+WQ specimens

CPT result, with corrosion damage following the profile of the deep, narrow surface grooves. The light grinding specimen with $R_a$ = 3.2 μm is shown in Fig. 3a with scattered pitting across the surface. The dimpled structure of the mill surface ($R_a$ = 3.5 μm) can be seen Fig. 3b, with the corrosion damage occurring along phase/grain boundaries at the bottom of dimples.

The conclusion of this study is that the surface roughness, $R_a$, is not enough on its own to judge the effect of the surface condition on the corrosion resistance of DSS components. This is in line with other recent studies [35] which conclude the same for other stainless steel grades. This is of practical importance to manufacturers and end users. Cutting tools, cold-drawing processes, surface grinding and handling produce a range of surfaces on the component prior to actual operation. Manufacturers should minimise the surface roughness as measured by $R_a$, but also consider manufacturing techniques that create narrow surface grooves. Surface parameters that measure the width of grooves, such as those described in [16], are required. Surface characterisation and prediction should be used to predict the effect of cutting and machining on the final surface produced [13–15]. Manufacturers and end users should examine final manufacturing surfaces using electrochemical assessments to establish expected in-service corrosion behaviour.

### 3.2 Microstructure variable

The heat treatment of the super duplex stainless steel for 30 min at 1,000°C and 1,300°C caused changes in both the microstructure and the corrosion resistance of the specimens compared with the solution-annealed material. The BSE and SEM observations of the 1,000°C specimen in Fig. 4 show the presence of intermetallic phases at the ferrite/austenite phase boundary. Figure 4a shows two different phases precipitated shown as light and darker grey against the near black austenite/ferrite background. Chemical analysis of the precipitates using EDX (shown in Fig. 5) confirmed the enrichment of the precipitated phases with Cr and Mo. The temperature range and high Cr content is in line with sigma ($\sigma$) phase, and the high Mo is characteristic of chi ($\chi$) phase [19–21]. Heat treatment at 1,300°C showed an increase in the volume fraction of ferrite phase and the formation of secondary austenite as shown in Fig. 6. The increase in ferrite volume fraction displaces nitrogen, allowing chromium nitrides $Cr_2N$ and chromium carbides $M_{23}C_6$ to form in the saturated ferrite. These act as initiation sites for the secondary austenite, but also deplete ferrite of chromium, leaving regions surrounding $Cr_2N$ precipitates with poor quality passive films and an increased susceptibility to localised corrosion damage.

The formation of sigma and chi phases had a detrimental effect on the corrosion resistance of the material. Figure 7 shows the pitting potentials ($E_p$) and protection potentials after cyclic sweep corrosion tests. The results demonstrate that both heat treatments and cooling regimes reduced the corrosion resistance of the material from around 600 mV Ag/AgCl for solution-annealed specimens to around 120 mV for the 1,000°C WQ specimens and 400 mV for the 1,300°C WQ. The rate of cooling also had an effect, increasing the amount of sigma phase and reducing $E_p$ in the 1,000°C specimens too. Slow cooling had the opposite effect on the 1,300°C AC specimens, allowing more secondary austenite to form and improving the corrosion resistance in the process. Evaluation of corrosion morphology of the 1,000°C WQ specimens using SEM revealed that the initiation of corrosion attack occurred preferentially at ferrite/austenite phase boundaries (shown in Fig. 8a) caused by the depletion of chromium and molybdenum in the material surrounding the precipitated phases. For 1,300°C specimens,

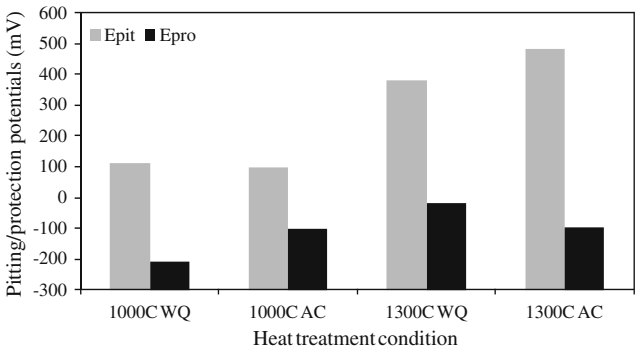


**Fig. 7** Heat treatment condition, pitting potentials and protection potentials of SDSS in 3.5% NaCl at 90°C

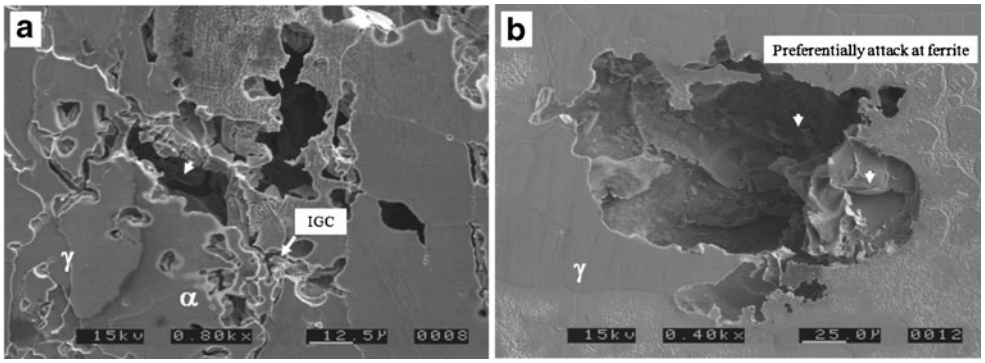


**Fig. 8** SEM corrosion morphology of heat treated specimens: **a** 1,000°C for 30 min+WQ, **b** 1,300°C for 30 min+WQ specimens

the corrosion damage was more pronounced in ferrite grains (shown in Fig. 8b), in line with the detrimental effect of $Cr_2N$.

The highly alloyed nature of the SDSS studied is responsible for its well-reported susceptibility to intermetallic precipitation at elevated temperatures [8, 9, 17]. The results of this study confirm that the thermo-mechanical treatment during manufacture is of critical importance to the corrosion resistance and final in-service performance of the material studied. Sigma and chi phases precipitate at 1,000°C, increasing in volume fraction with exposure time. The results of the air-cooled specimens suggest similar precipitation behaviour to other 25Cr–07Ni SDSS grades, and temperatures within the range 800–1,000°C should be avoided during the manufacturing route, welding and operational conditions through good temperature control and fast quenching procedures [17]. High-temperature exposure of 1,300°C+ should also be avoided, but slow cooling should be used to allow secondary austenite to form, alleviating the effects of the chromium nitrides formed. Other SDSS grades or differently manufactured materials should be assessed for sensitivities to temperature and time and the final microstructure assessed for the presence of sigma and chi phases using either metallographic analysis or non-destructive techniques such as those described in [36]. Manufacturers and end users should assess the effect of the specific manufacturing routes and welding procedures on the corrosion resistance of individual products and not rely on traditional material selection procedures or specimens prepared using standard methods. The emphasis should be on assessing finished component microstructures.

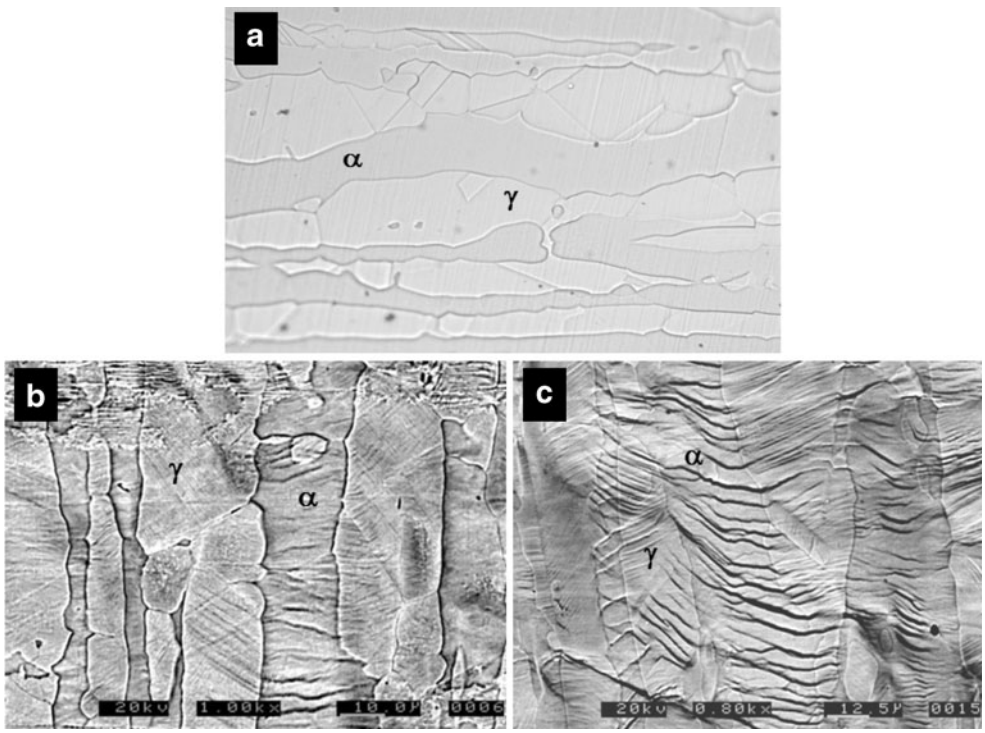


**Fig. 9** Photographs of free/cold-worked SDSS: **a** solution annealed, **b** 8%plastic strain, **c** 16%plastic strain

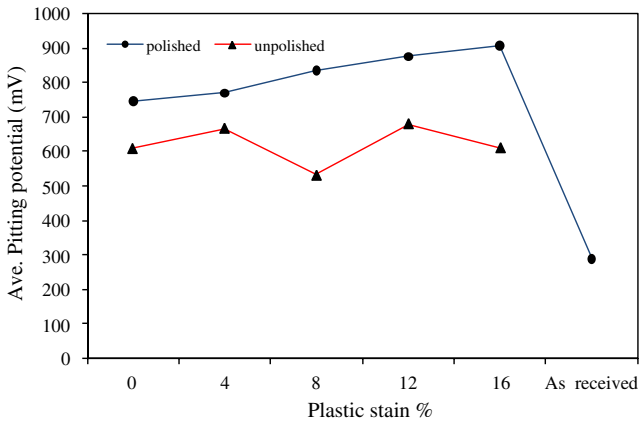


**Fig. 10** Pitting corrosion vs plastic strain percentage of SDSS

### 3.3 Plastic deformation (cold work) variable

The mechanical, metallographic and corrosion analyses of the SDSS specimens at the five different cold work levels of 0%, 4%, 8%, 12% and 16% plastic strain were carried out and the results recorded. Examples from the metallographic changes after cold work are shown in Fig. 9. The materials acquired deformation bands on the external surface and through the internal structure. The deformation marks on the ferrite and austenite phases are seen in the BSE images in Figs. 9b, c. These are in agreement with those reported [37, 38]. The deformations had a major impact on the corrosion resistance and the hydrogen embrittlement susceptibility of the super duplex stainless steel investigated.

The pitting potentials retrieved from the polarisation curves of the pre-deformed longitudinal and polished transverse specimens were recorded. The results for each specimen type were averaged and the results presented in Fig. 10. The corrosion resistance of the specimens with the surface deformations was slightly improved by 4% plastic strain and then drastically decreased at 8% plastic strain. A slight improvement in the pitting corrosion potential of 12% $\varepsilon_{pl}$ specimens was also observed before the pitting potential dropped again after 16% $\varepsilon_{pl}$. The results show that the surface and subsurface deformation structures on SDSS specimens have a nonlinear impact on corrosion resistance with increasing plastic strain. Some strain levels caused no change compared with the solution-annealed material, whilst others cause major reductions (8% and 16% $\varepsilon_{pl}$). A similar nonlinear relationship between corrosion resistance and increasing cold work in a duplex stainless steel was also reported by Takizawa et al. [34].

The pitting potential results of the polished transverse surfaces show a different trend. Once the surface deformations had been removed, cold work had a beneficial effect on the corrosion resistance of the material. The pitting corrosion resistance improved as the cold work increased gradually from 4% to 16% plastic strain. The as-received specimens, which have been cold-drawn at manufacture, showed the lowest pitting corrosion potential. This suggests that there is a critical level of cold work beyond which there is a detrimental impact on the corrosion resistance of the material. This behaviour of the subsurface material is in agreement with the effect of cold work on corrosion resistance of austenitic grades reported in [39]; however, other studies suggest a decrease [40]. It is clear from the results of this study that the former is the case for the SDSS studied.

The corrosion morphology (shown in Fig. 11) gives insight into the physical phenomenon occurring. The deformation bands on the pre-strained surfaces worked as corrosion initiation sites for pitting corrosion. This effect is more pronounced as the cold work is increased to 16% $\varepsilon_{pl}$. Increasing cold work reduced the ferrite phase corrosion

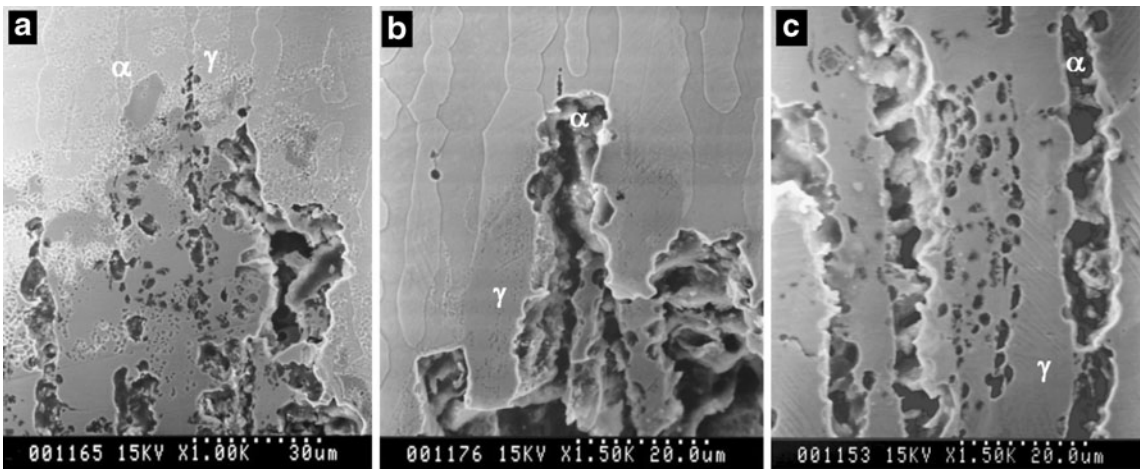


**Fig. 11** Corrosion morphologies on SDSS surfaces after corrosion test in 3.5% NaCl at 90°C: **a** solution-annealed specimen, **b** 8%plastic strain specimen, **c** 16%plastic strain specimen

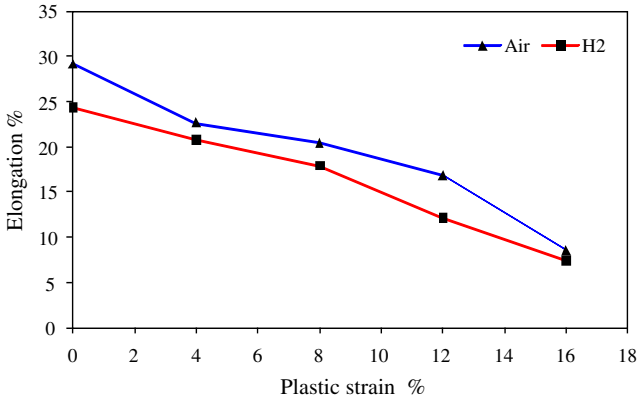


**Fig. 12** Effect of hydrogen charging and cold work on elongation to failure of SDSS

resistance as evidenced by the increasing dissolution of ferrite, whilst the austenite suffered from clusters of localised pitting. The results demonstrate that the effect of cold work on the corrosion resistance of SDSS is a complex issue. If the manufacturing process allows deformation bands to form at the surface, certain critical plastic strains can cause large reductions in the corrosion resistance, whilst manufacturing processes that remove these deformation structures could leave finished cold-worked products with improved resistance. The extent of cold work, the use of surface treatments and the method of determining surface topography [41] should therefore be considered carefully by manufacturers and final component performance again assessed.

Cold work was also found to have an effect on the mechanical properties when the alloy was charged with hydrogen in 0.1 M $H_2SO_4$ at room temperature. The effect of plastic strain and hydrogen charging on elongation to failure is shown in Fig. 12. The results showed that the increase in cold work reduced the ductility of the material, with elongation to failure decreasing from 29.19% when the specimen was free of cold work to 22.38%, 20.44%, 16.94% and 8.93% after cold work was applied at 4%, 8%, 12% and 16% $\varepsilon_{pl}$, respectively. The addition of hydrogen to the SDSS alloy reduced its ductility further. The elongation to failure reduced from 29.19% for the free hydrogen specimen to 24.84% after 48 h hydrogen charging. The effect of hydrogen on the material's ductility increased from 4% onwards, peaking at 12% $\varepsilon_{pl}$, as shown in Fig. 12. This was a result of the increasing number of hydrogen traps in the material with increasing cold work and the effect of the cold work on the specimen's passive film. The experimental results are in agreement with Huang et al. [42] who confirmed that cold work results in a decrease in diffusivity of hydrogen in steel. This implies an increase in the solubility of hydrogen in the steel, and the authors have suggested that cold work increases hydrogen uptake. This increase often has a detrimental effect on the material's mechanical properties, such as crack resistance and notch tensile strength [43, 44].

The fracture morphology of the hydrogen free specimen is shown in Fig. 13a, with classical ductile fracture behaviour visible. The fracture morphology after hydrogen charging shows a region of brittle cleavage fracture extending from the surface towards the centre of the specimen. The depth of the brittle region increased with increasing cold work, as did the severity of the secondary cracks on the external surface shown in Fig. 13b,c. Hydrogen saturation created the appearance of secondary cracks on the outer surface of the samples, as shown in SEM images in Fig. 14a. Figure 14b shows high magnification on the fracture surfaces within the depth of the secondary cracks. The average depth of the brittle zone as a function of plastic strain was calculated from the images and the results reported in Fig. 15, confirming the detrimental effect of cold work on the material's resistance to hydrogen embrittlement [45].

The investigation into the effect of cold work on the corrosion resistance of SDSS revealed a complex series of positive and negative results. Whilst increasing cold work

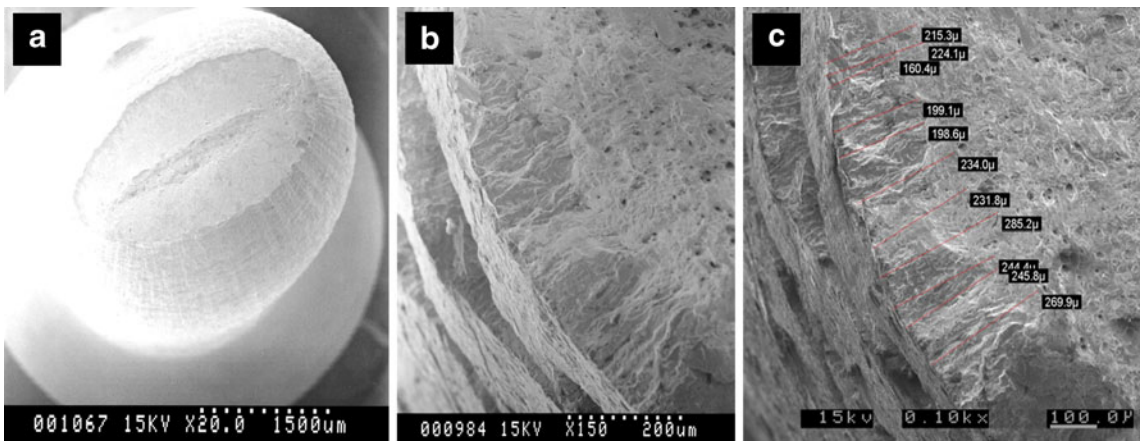


**Fig. 13** Difference in fracture surface between air and hydrogen charged specimens: **a** air, **b** 48 h hydrogen charging, **c** brittle region depth

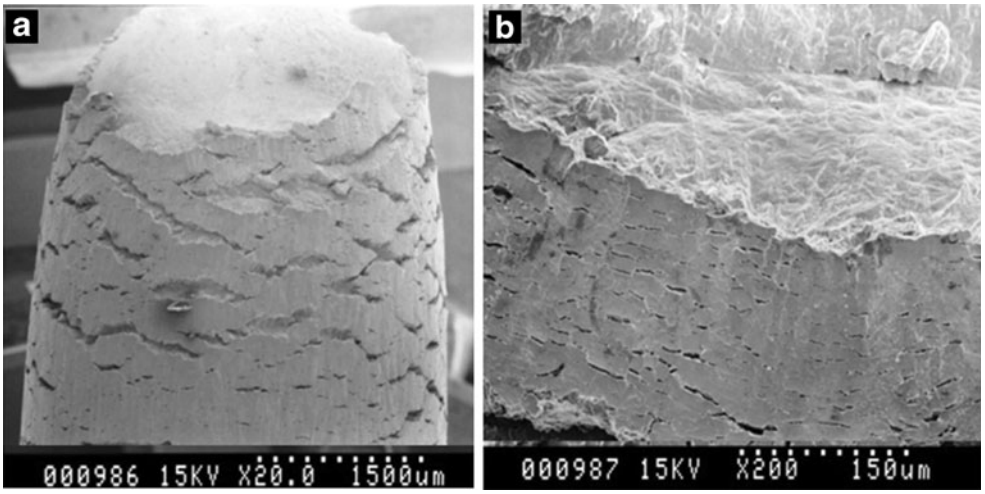


**Fig. 14** Secondary cracks: **a** external surface, **b** interior surface of secondary crack

can improve the material's corrosion resistance, this is only achieved if surface deformation structures are not allowed to form or are removed. However, the gain in corrosion resistance in chloride-bearing solutions is at the expense of an increase in susceptibility to hydrogen embrittlement. Surface treatment, for example shot peening, could be of benefit provided that the effect of the shot parameters was carefully analysed, as it was for grade 316 in [46]. A similar study on surface treatments would be of benefit for the duplex grades. Manufacturers and end users must consider the decision on the degree of cold work to apply as a set of compromises on component strength, corrosion resistance, and hydrogen embrittlement and tailor the result for specific applications.

## 4 Conclusions

After the in-depth study of the UNS S39274 super duplex stainless steel using conventional electrochemical corrosion techniques, the following final conclusions can be drawn on the effects of the manufacturing variables studied:

### 4.1 Surface condition

- Surface condition has a significant role in the corrosion resistance of the steel. The critical pitting temperature and pitting potential determination are good methods for distinguishing between the corrosion resistances of SDSS surfaces.
- Relying on the surface roughness parameter, $R_a$, alone is not recommended for the prediction of surface corrosion behaviour. The effect of narrow and deep scratches cannot be characterised by $R_a$, and more detailed surface topology measurement should be used along with electrochemical assessment of specific manufactured surfaces.
- The surface topography controls the corrosion morphology and the severity of the corrosion damage. The effect of manufacturing processes on surface condition should be carefully monitored for SDSS components.

### 4.2 Microstructure and heat treatment

- Changes in microstructure occur when SDSS specimens are exposed to high temperatures, and these can have a significant effect on the corrosion resistance. Exposing this alloy to temperature of 1,000°C for 30 min leads to the precipitation of sigma ($\sigma$) and chi ($\chi$) intermetallics.
- The existence of these intermetallic phases weakened the resistance to intergranular and pitting corrosion. The pitting potential for solution-annealed material free of sigma and chi intermetallics was 600 mV Ag/AgCl. This value was reduced to 112 mV Ag/AgCl for 1,000°C microstracture containing the intermetallics.
- Exposing this alloy to 1,300°C leads to an increase in the volume fraction of ferrite phase and the formation of secondary austenite. The corrosion resistance was

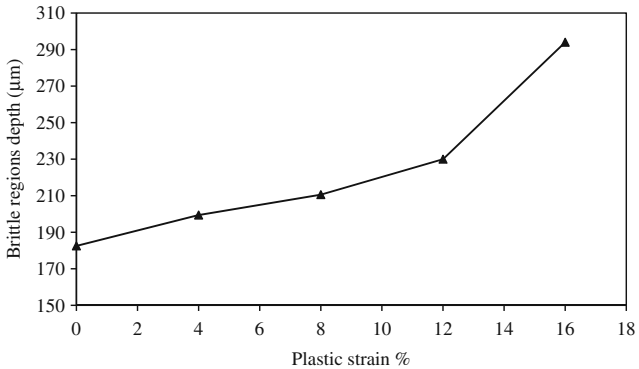


**Fig. 15** Average of brittle depth region of cold-worked specimens after 48-h hydrogen charging in 0.1 M $H_2SO_4$

reduced when compared with the solution-annealed material, but not to the same extent as the 1,000°C specimens.

### 4.3 Plastic deformation and cold work

- Cold working the SDSS alloy led to the presence of deformation structures on the surface. The ferrite experiences multiple types of defromation bands. Increasing the amount of cold work to 16% increased the deformation bands.
- Effect of cold work on the corrosion resistance of the unpolished specimens showed an irregular effect. It was beneficial in some cases whilst in other cases is harmful. This was explained by a nonlinear development of the defromation bands and changes in the surface structure of both phases.
- Cold work improved the pitting corrosion resistance of the polished surfaces up to a certain critical amount of plastic strain.
- The susceptibility of the alloy to hydrogen embrittlement was increased by cold work; the greater the degree of cold work, the greater are the changes in the mechanical properties.
- Increasing cold work increased the depth of the brittle region as well as the intensity of secondary cracks on the surface. The average depth of SDSS material affected by hydrogen increased from 182.51 μm at no pre-strained specimens to 294 μm at 16%plastic strain specimen.

Manufacturers and end users should consider how the manufacturing variables will effect the performance of SDSS grades in specific applications.

**Acknowledgements** The authors would like to thank the Gaddafi International Charity and Development Foundation (GICDF) for the financial support of this research which has been carried out at the University of Aberdeen, UK.

## References

1. Mowat DE, Edgerton MC, Wade EHR (2002) Erskine field HP/HT workover and tubing failure investigation. J Petrol Technol 53 (3):68–71
2. Hannah IM, Seymour DA (2006) Shearwater super duplex tubing failure investigation. Corrosion NACE, Paper No. 06491
3. Sentence P (1991) Hydrogen embrittlement of cold worked duplex stainless steel oilfield tubulars. Duplex stainless steel 91, 28–30 October, Beaune Bourgogne, France
4. Linton V, Laycock N, Keen D, Boon P (2008) SCC failure of a super duplex separator vessel in an ammonium nitrate plant. Materials Performance 47(9):64–68
5. Elshawesh F, Elhoud A, Ragha O (2001) Role of surface finish and post-fabrication cleaning on localized corrosion of 316 L austenitic stainless steel flash chambers. Eurocorr 2001, Riva del Garda, Italy, September 30–October 4
6. Burstein GT, Vines SP (2001) Repetitive nucleation of corrosion pits on stainless steel and the effects of surface roughness. J Electrochemi Soc 148(12):B504–B516
7. Oberndorfer M, Thayer K, Kastenbauer M (2004) Application limits of stainless steels in the petroleum industry. Mater Corros 55(3):174–180
8. Charles J (1991) The duplex stainless steels: materials to meet your needs. Proc Duplex Stainless Steels 91:10–17
9. Nilsson JO (1992) Overview: super duplex stainless steel. Mater Sci Technol 8(8):686–700
10. Pistorius PC, Burstein GT (1992) Metastable pitting corrosion of stainless steel and the transition to stability. Philos Trans R Soc Lond A341:531–559
11. Sasaki K, Burstein GT (1996) The generation of surface roughness during slurry erosion–corrosion and its effect on the pitting potential. Corrosion Science 38(12):2111–2120
12. Hong T, Nagumo M (1997) Effect of surface roughness on early stages of pitting corrosion of type 301 stainless steel. Corrosion Science 39(9):1665–1672
13. Wang X, Feng CX (2002) Development of empirical models for surface roughness prediction in finish turning. Int J Adv Manuf Technol IJAMT 20(5):348–356. doi:10.1007/s001700200162
14. Benardos PG, Vosniakos G (2003) Predicting surface roughness in machining: a review. Int J Adv Manuf Technol IJAMT 43(8):833–844. doi:10.1016/S0890-6955(03)00059-2
15. Singh D, Venkateswara Rao P (2007) A surface roughness prediction model for hard turning process. Int J Adv Manuf Technol 32:1115–1124. doi:10.1007/s00170-006-0429-2
16. Gadelmawla ES, Koura MM, Maksoud TMA, Elewa IM, Soliman HH (2002) Roughness parameters. J Mater Process Technol 123 (1):133–145. doi:10.1016/S0924-0136(02)00060-2
17. Chen TH, Weng KL, Yang JR (2002) The effect of high-temperature exposure on the microstructural stability and toughness property in a 2205 duplex stainless steel. Mater Sci Eng A 338(1–2):259–270. doi:10.1016/S0921-5093(02)00093-X
18. Atxaga G, Irisarri AM (2009) Study of the failure of a duplex stainless steel valve. Eng Fail Anal 16:1412–1419
19. Hitchcock GR, Deans WF, Thompson DS, Coats A (2001) Pin-hole and crack formation in a duplex stainless steel downhole tool. Eng Fail Anal 8:213–226
20. Takizawa K, Shimizu T, Yoneda E, Tamura I (1982) Effect of cold work, heat treatment and volume fraction of ferrite on stress corrosion cracking behaviour of duplex stainless steel. Transactions of the Iron and Steel Institute of Japan ISIJ 22:325–332
21. Herting G (2004) Metal release from stainless steels and the pure metals in different media. Licentiate thesis, Royal Institute of Technology, Stockholm, p 2
22. Schwind M, Kallqvist J, Nilsson JO, Agren J, Andren HO (2000) σ-Phase precipitation in stabilized austenitic stainless steels. Acta Mater 48:2473–2481
23. Atamert S, King JE (1993) Sigma-phase formation and its prevention in duplex stainless steels. J Mater Sci Lett 12(14): 1144–1147
24. Symniotis E (1995) Dissolution mechanism of duplex stainless steels in the active-to-passive transition range and the role of microstructure. Corrosion 51(8):571–580
25. Yang SW, Spruiel JE (1982) Cold-worked state and annealing behaviour of austenitic stainless steel. J Mater Sci 17(3):677–690
26. Elayaperumal K, De PK, Balachandra J (1972) Passivity of type 304 stainless steel—effect of plastic deformation. Corrosion 28 (7):269–273
27. Randak A, Trautes FW (2004) Influence of austenite stability of 18-8 Cr–Ni-steels on the cold working and corrosion properties of these steels. Mater Corros 21(4):79

28. Bernhardsson S (1991) The corrosion resistance of duplex stainless steels. Conference Proceeding of Duplex Stainless Steels '91, vol 1, p 185, Bourgogne, France
29. Chou SL, Tsai WT (1999) Effect of grain size on the hydrogen-assisted cracking in duplex stainless steels. Mater Sci Eng A270:219–224
30. Coussement C, Fruytier D (1991) An industrial application of duplex stainless steel in the petrochemical industry: a case study, failure analysis and subsequent investigations. Duplex Stainless Steels 91:521–529
31. ASTM (1997) ASTM designation: G 150-97: Standard method for electrochemical critical pitting temperature testing of stainless steels. American Society for Testing and Materials
32. Brigham RJ, Tozer EW (1973) Temperature as a pitting criterion. Corrosion 29:33
33. Moayed MH, Laycock NJ, Newman RC (2003) Dependence of the critical pitting temperature on surface roughness. Corros Sci 45:1203–1216
34. Burstein GT, Pistorius PC (1995) Surface roughness and the metastable pitting of stainless steel in chloride solutions. Corrosion 51(5):380–385
35. Faller M, Buzzi S, Trzebiatowski OV (2005) Corrosion behaviour of glass-bead blasted stainless steel sheets and other sheets with dull surface finish in a chloride solution. Materials and Corrosion 56(6):373–378
36. Normando PG, Moura EP, Souza JA, Tavares SSM, Padovese LR (2010) Ultrasound, eddy current and magnetic Barkhausen noise as tools for sigma phase detection on a UNS S31803 duplex stainless steel. Materials Science and Engineering A 527 (12):2886–2891. doi:10.1016/j.msea.2010.01.017
37. Serre I, Salazar D, Vogt J-B (2008) Atomic force microscopy investigation of surface relief in individual phases of deformed duplex stainless steel. Mater Sci Eng A 492:428–433
38. Fréchard S, Martin F, Clément C, Cousty J (2006) AFM and EBSD combined studies of plastic deformation in a duplex stainless steel. Mater Sci Eng A 418:312–319
39. Kamachi MU, Shankar P, Ningshen S, Dayal RK, Khatak HS, Raj B (2002) On the pitting corrosion resistance of nitrogen alloyed cold worked austenitic stainless steels. Corros Sci 44(10):2183–2198
40. Barbucci A, Cerisola G, Cabot PL (2002) Effect of cold working in the passive behaviour of 304 stainless steel in sulfate media. J Electrochem Soc 149(12):B534–B542
41. Vorburger TV, Rhee H-G, Renegar TB, Song J-F, Zheng A (2007) Comparison of optical and stylus methods for measurement of surface texture. Int J Adv Manuf Technol 33(1–2):110–118. doi:10.1007/s00170-007-0953-8
42. Huang Y, Nakajim A, Nishikata A, Tsuru T (2003) Effect of mechanochemical deformation on permeation of hydrogen in iron. Transactions the Iron and Steel Institute of Japan ISIJ 43(2):548–554
43. Tsubankino H, Ando A, Masuda T, Yamakawa K (1985) Hydrogen attack produced by an electrochemical method using molten salts. Transactions the Iron and Steel Institute of Japan ISIJ 25(9):999–1001
44. Asahi H, Ueno M (1993) Effect of cold-working on sulfide stress cracking resistance of low alloy martensitic steels. Transactions the Iron and Steel Institute of Japan ISIJ 33(12):1275–1280
45. Elhoud AR, Renton NC, Deans WF (2010) Hydrogen embrittlement of super duplex stainless steel in acid solution. Int J Hydrogen Energy 35(12):6455–6464. doi:10.1016/j.ijhydene.2010.03.056
46. Mahagaonkar SB, Brahmankar PK, Seemikeri CY (2008) Effect of shot peening parameters on microhardness of AISI 1045 and 316 L material: an analysis using design of experiment. Int J Adv Manuf Technol 38(5–6):563–574. doi:10.1007/s00170-007-1222-6